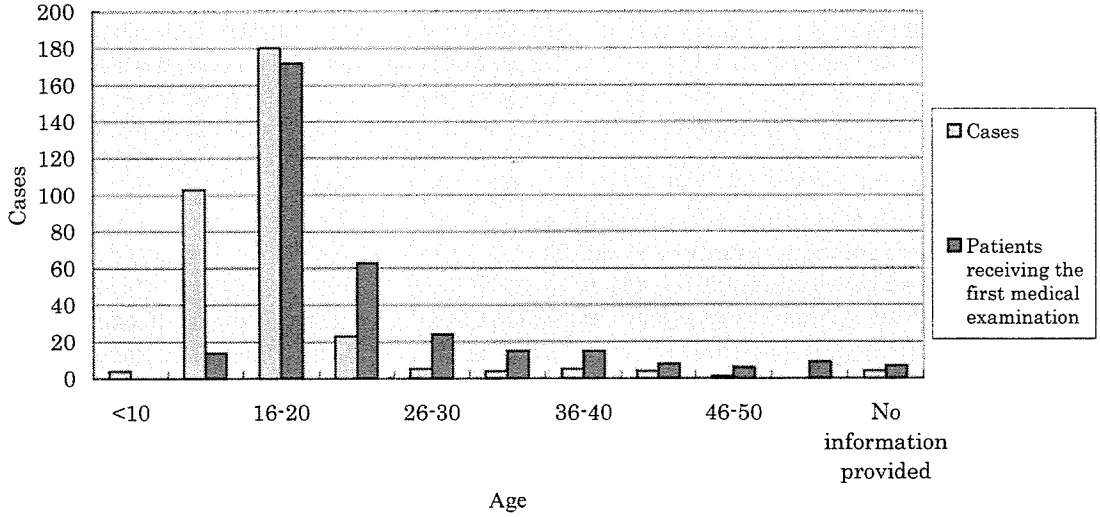

Figure 1. Distribution of ages at onset, and ages of patients at first neurological examination.

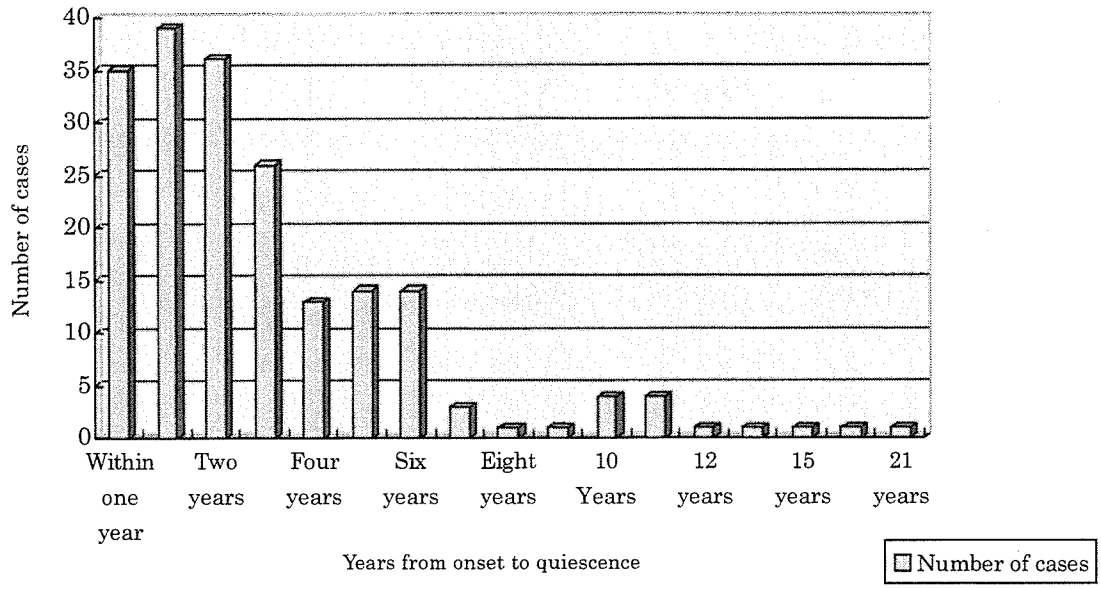

Figure 2. Time lapse between onset and quiescence.

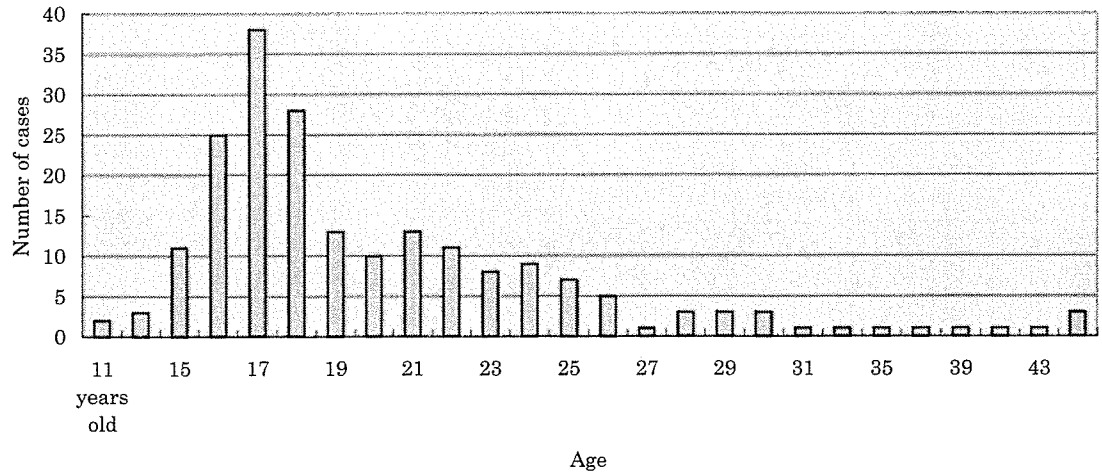

Figure 3. Ages of patients in the quiescent stage.

Table IV. Neurological findings.

Muscular atrophy	Found	Not found	Unknown	No information provided
1. Hand muscles	296	6	2	8
2. Distal parts of the forearm, the ulnar side of the forearm	251	32	15	13
3. Brachioradial muscle	51	228	18	14
4. Biceps brachii	25	259	14	13
5. Triceps brachii	49	234	14	14
6. Other	18	144	10	140
Cold paresis	205	55	65	8
Trembling of fingers	221	73	31	8
Fascicular twitching	101	168	46	18
Other				
1. Sensory disturbance	64	259	2	8
2. Tendon reflex abnormality	127	191	4	11
3. Babinski sign	7	280	24	22

content of the dura were the main findings. The only autopsy case revealing neuropathological findings in the spinal cord was that reported by Hirayama et al. (6) (see above).

Neuroradiological findings

Plain cervical spine radiographs were available; in 29 cases the neck was unusually straight, in 30 cases there was angulation of the neck, in 26 cases there was a bony spur, and in 11 cases there was a degree of subluxation.

Myelography , CT myelography, and cervical cord MRI were performed in 185, 171, and 229 cases, respectively, revealing atrophy, flattening, forward displacement of the cervical cord, forward displacement of posterior dura and expansion of the posterior epidural space in a large number of cases examined. Asymmetrical atrophy of the cervical cord was seen in most cases. A summary of the findings is given in Table V.

Whatever the imaging methods used, forward displacement of the cervical cord was the most frequently observed abnormality. The number of years from the first neurological examination to neuroradiological examinations was evaluated in relation to the presence or absence of forward displacement of the posterior wall of the dural tube in 136 cases. Forward displacement of the posterior wall of the dural tube was found by myelography, CT after myelography, MRI, or combinations of these methods (Figure 4), but these data suggest that dural displacement diminishes within several years of onset of the illness.

Electrophysiological findings

EMG was conducted in 265 of 333 cases. Information on the findings was available in 245 cases, showing abnormalities suggestive of neurogenic changes in 241 out of 245 cases (98.4%). In 70 of 95 cases there were EMG abnormalities even in clinically unaffected limbs (73.7%). This supports the finding reported in the past that limbs with no apparent symptoms of JMADUE could show abnormality by EMG. Nerve conduction velocity was measured in some cases, but no significant abnormality was noted.

Cerebrospinal fluid findings

CSF findings included normal protein in 142 cases, abnormal in 9 cases, and unknown in 6 cases, but the details of the abnormalities were not described in the survey form.

Table V. Abnormal findings of cervical cord and dura mater on neuroradiological examinations.

	Myelography (185 cases)	CT after myelography (171cases)	MRI (sagittal section) (229 cases)	MRI (horizontal section) (229 cases)
Atrophy of cervical cord	65%	83%	65%	75%
Flattening of cervical cord	72	86	76	77
Forward displacement of cervical cord	86	88	81	81
Forward displacement of posterior wall of dural tube	74	75	68	69
Expansion of posterior extradural space		-	73	

Percentage figures were calculated as follows: [% of cases in which findings were reported/(% of cases in which abnormal findings were reported+% of cases in which abnormal findings were not reported)] $\times 100$.

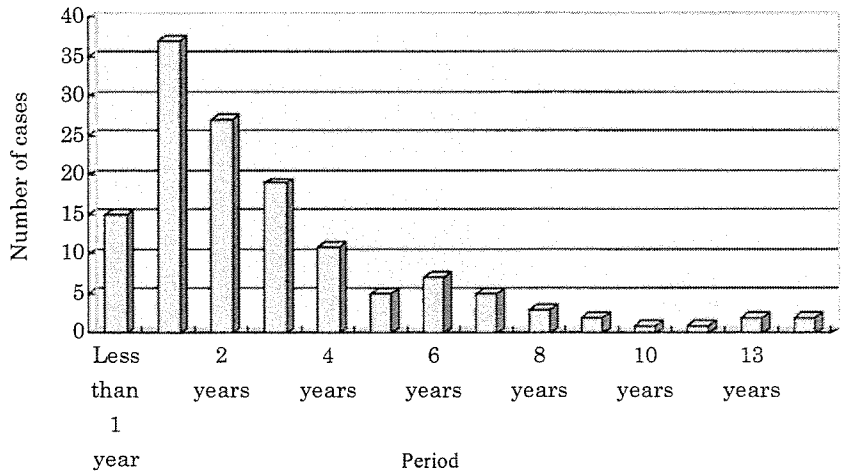

Figure 4. The number of cases of forward displacement (+) of the posterior wall of the dural tube plotted with respect to the period from onset to neurological examination.

Treatment

The effectiveness of cervical collar immobilization was evaluated in 56 cases. This management proved effective in 32 of 56 cases (57.2%). Based on the neuroradiological findings showing forward displacement of cervical cord and of the posterior wall of the dural tube as shown in Table V, the positive effects of cervical collar immobilization was intuitively a reasonable therapeutic method. As for surgical treatments, various surgical techniques were used in 41 cases to restrict the forward flexion of the cervical spine or to permit the dura mater to relax. The information provided in this survey, although necessarily subjective, suggested that all these techniques showed favorable therapeutic effects.

Discussion

In the present survey, the majority of cases were reported from 10 hospitals with neurology departments. Cases reported by these hospitals numbered 240 out of 333 in total, comprising 72% of all the cases reported to us. These neurology departments are well known for the diagnosis and treatment of JMADUE (Hirayama disease). It is presumed, therefore, that other hospitals with little experience in treating this disease might have referred their patients to these hospitals, so that it was unnecessary to return the survey forms to the secretariat from these primary hospitals. The quite low response rate to our initial inquiry could thus be explained.

A review of the numbers of JMADUE cases diagnosed each year shows that the number of patients with this diagnosis has been increasing in recent years (Table II), probably due to increasing recognition of JMADUE.

It has been observed that young people today in Japan are taller than in previous times. Therefore, it can be estimated that the rate of growth in adolescence has increased, and we may wonder whether JMADUE is due to a resulting imbalance between the development of the spinal column and that of the spinal cord (32,34).

The overwhelming majority of patients with JMADUE are males (281 to 34). Regardless of ethnicity, the height of females begins to increase earlier than that of males. Once males begin to increase in height, however, they increase quickly and eventually exceed the height of females. An imbalance between development of the spinal column and that of the spinal cord, which is assumed to be the cause of JMADUE, may be related to the male's pattern of height increase (32). JMADUE appears in females later than in males. This difference in age at onset by gender might also be related to gender-related differences in the effect of sex hormones on motor neurons. The early atrophy observed in hand muscles and the distal ulnar side of the forearm was designated as 'oblique amyotrophy' by Hirayama, because the part affected by atrophy is clearly distinguishable from the brachioradialis muscle, which is usually unaffected (32).

In the present survey, only two familial cases were reported: two pairs of brothers. Familial cases are extremely rare, and JMADUE appears usually to be a sporadic disease. As for the patho-mechanism of this entity, Yada et al. proposed in 1982 the theory 'over-stretch mechanism of cervical cord' such that the myelopathy could be caused by a relative imbalance between the cervical vertebrae and the cervical cord (40). Significant advances in elucidating the pathophysiology of JMADUE were made possible by neuroradiological studies. Mukai et al. in 1985 (35) used myelography to study the cervical cords of patients with JMADUE, and reported that there was flattening of the lower cervical cord and forward displacement of the posterior wall of the dural tube in the forward flexed posture. This report broke the ground for important studies made in

following years. Kikuchi et al. pursued their study from the standpoint of biomechanics, and in 1987 they proposed the term 'flexion myelopathy with tight dural canal inflexion' (36). In JMADUE, the lower cervical cord becomes displaced forward, comes into contact with the posterior surface of the vertebral body, and becomes flattened when the cervical spine flexes forward (flexion myelopathy). If this happens, the posterior wall of the dural tube also becomes displaced forward in most cases, so that pressure is exerted on the spinal cord (tight dural canal in flexion). CT and MRI procedures verify that the posterior extradural space expands during forward flexion of the cervical vertebrae due to the expanded venous plexus. Such a finding was also observed in many cases reported by Tokumaru and Hirayama (33,37). On the other hand, patients with forward displacement and flattening of the cervical cord without displaced dura also occur. This means that there are cases in which the cervical cord is displaced and flattened during forward flexion of the cervical spine, without forward displacement of the posterior wall of the dural tube. Hirayama and Tokumaru reported that the displacement of the wall of the dura mater decreases as the patient grows older (33,37), but some researchers argue for the existence of a subtype of JMADUE that does not exhibit displacement in the wall of the dura mater in the early to later stages of the disease. Whether the cervical spine is fully flexed or not is the important point to be considered if we are to evaluate forward displacement of the posterior wall of the dural tube correctly. The patient may have difficulty in flexing the cervical spine forward properly, because of restrictions in mobility within most CT equipment, a factor that is even more relevant in MRI equipment. Hirayama and Tokumaru obliquely raised the patient body using special seating to allow the patient to flex the cervical spine sufficiently (33). Thus they were able to obtain correct imaging data. This means that if the cervical spine could be flexed properly, the actual number of cases in which forward displacement of the posterior wall of the dural tube occurred might be much larger. Our survey form did not include data on somatosensory evoked potential (SEP) and magnetic evoked potentials (MEP), but data have been reported by Kikuchi and Tashiro (38).

Based on the theory of cervical flexion myelopathy, surgical cervical fusion has been proposed (41). Cervical collars were used and proved effective in many cases. The use of cervical collars not only stopped the progress of the disease, but also alleviated the muscular atrophy and weakness in some cases (42,43). This therapy has already become a well-established approach in Japan. Considering that early detection and early treatment by using conservative methods are effective in preventing it from progressing, it is important to enlighten people on JMADUE, and the necessity for early detection should be emphasized.

Conclusion

Three hundred and thirty-three cases of JMADUE (Hirayama disease) were identified by a nationwide survey in Japan. We propose the importance of worldwide recognition of JMADUE as a unique upper limb distal amyotrophy, clinically distinct from other amyotrophies, especially motor neuron disease. Since gradually increasing numbers of case reports on Hirayama disease have appeared outside Japan, this disease may not be such a rare entity or a disorder only affecting the Japanese. We encourage further international studies. The clinical laterality and age at onset, the mechanism of upward/downward shift (overstretch) of cervical cord, and forward displacement of the dural tube are important concepts.

References

1. Hirayama K, Toyokura Y, Tsubaki T. Juvenile muscular atrophy of unilateral upper extremity; a new clinical entity. Psychiatr Neurol Jpn. 1959;61:2190–7.(In Japanese, abstract in English.)
2. Hirayama K, Tsubaki T, Toyokura Y, Okinaka S. Juvenile muscular atrophy of unilateral upper extremity. Neurology. 1963;13:373–80.
3. Hirayama K. Juvenile non-progressive muscular atrophy localized in the hand and forearm – observations in 38 cases. Rinsho Shinkeigaku. 1972;12:313–24. (In Japanese, abstract in English.)
4. Sobue I, Saito M, Iida M, Ando K. Juvenile type of distal and segmental muscular atrophy of upper extremities. Ann Neurol. 1978;3:429–32.
5. Gourie-Devi M, Suresh TG, Shankar SK. Monomelic amyotrophy. Arch Neurol. 1984;4:388–94.
6. Hirayama K, Tomonaga M, Kitano K, Yamada T, Kojima S, Arai K. Focal cervical poliopathy causing juvenile muscular atrophy of distal upper extremity: a pathological study. J Neurol Neurosurg Psychiatry. 1987;50:285–90.
7. Hirayama K. Non-progressive juvenile spinal muscular atrophy of the distal upper limb (Hirayama's disease). In: Vinken PJ, Bruyn GW, Klawans HL, editors. Disease of the motor system. Handbook of Clinical Neurology. Vol. 15(59) Amsterdam: Elsvier; 1991. pp 107–20.
8. Loong SC, Yap MHL, Nei IP. An unusual form of motor neuron disease. In: Fourth Asian and Oceanic Congress of Neurology, 16–21 November 1975, Sompon Press, Abstr 35.
9. Singh N, Sachdev KK, Susheela AK. Juvenile muscular atrophy localized to arms. Ann Neurol. 1980;37:297–9.
10. Tan CT. Juvenile muscular atrophy of distal upper extremities. J Neurol Neurosurg Psychiatry. 1985;48:285–6.
11. Virmani V, Mohan PK. Non-familial, spinal segmental muscular atrophy in juvenile and young subjects. Acta Neurol Scand. 1985;72:336–40.
12. Peiris JB, Senevirante KN, Wickremashighe HR, Gunatilake SB, Gamage R. Non-familial juvenile distal spinal muscular atrophy of upper extremity. J Neurol Neurosurg Psychiatry. 1989;52:314–9.
13. Chan YW, Kay R, Schwartz MS. Juvenile distal spinal muscular atrophy of upper extremities in Chinese males: a single fiber electromyographic study of arms and legs. J Neurol Neurosurg Psychiatry. 1991;54:165–6.

14. Kao KP, Wu ZA, Chen CM. Juvenile lower cervical spinal muscular atrophy in Taiwan: report of 27 Chinese cases. Neuroepidemiology. 1993;12:331–5.
15. Mirsa UK, Kalita J. Central motor conduction in Hirayama disease. Electroencephalogr Clin Neurophysiol. 1995;97: 73–6.
16. Chen CJ, Chen CM, Wu CL, Ro LS, Chen ST, Lee TH. Hirayama disease: MR diagnosis. AJNR Am J Neuroradiol. 1998;19:365–8.
17. Pilgaard S. Unilateral juvenile muscular atrophy of upper limb. Acta Orthop Scand. 1968;39:327–31.
18. Compernolle T. A case of juvenile muscular atrophy confined to one upper limb. Eur Neurol. 1973;10:237–42.
19. Adornato T, Engel W, Kucera J, Bertorini TE. Benign focal amyotrophy. Neurology. 1978;28:399 (Abstract).
20. O'Sullivan DJ, McLeod JG. Distal chronic spinal muscular atrophy involving the hands. J Neurol Neurosurg Psychiatry. 1978;41:653–8.
21. Harding AE, Bradbury PG, Murray NMF. Chronic asymmetrical spinal muscular atrophy. J Neurol Sci. 1983;59:69–83.
22. Schlegel U, Jerusalem F, Tackmann W, Cordt A, Tsuda Y. Benign juvenile focal muscular atrophy of upper extremities: a familial case. J Neurol Sci. 1987;80:351–3.
23. Leys D, Petit H. Amyotrophie juvénile distale chronique unilatérale localisée à un member supérieur (type Hirayama): un cas européen.. Rev Neurol. 1987;143:611–3.
24. Chaine P, Bouche P, Léger JM, Dormont D, Cathala HP. Atrophie musculaire progressive localisée à la main. Forme monomelique de maladie du motoneurone? Rev Neurol. 1988;144:756–63. (Abstract in English.)
25. Gaio JM, Lechevalier B, Hommel M, Viader F, Chapon F, Perret J. Atrophie spinale chronique des members supérieurs de l'adulte jeune (syndrome de O'sullivan et McLeod). Rev Neurol. 1989;145:163–8. (Abstract in English.)
26. Biondi A, Dormont D, Weitzer I Jr, Bouche P, Chaine P, Bories J. MR imaging of the cervical cord in juvenile amyotrophy of distal upper extremity. AJNR Am J Neuroradiol. 1989;10:263–8.
27. Oryema J, Ashby P, Spiegel S. Monomelic atrophy. Can J Neurol Sci. 1990;17:124–30.
28. Donofrio PD. Monomelic amyotrophy. Muscle Nerve. 1994;17:1129–34.
29. Billé-Turc , Billé J, Azulay JPH, Padovani R, Serratrice G. La maladie d'Hirayama: maladie ou syndrome? Rev Neurol. 1996;152:20–6. (Abstract in English.)
30. Drozdowski W, Baniukiewicz E, Lewonowska M. Juvenile monomelic amyotrophy: Hirayama disease. Neurol Neurochir Pol. 1998;32:943–50. (Abstract in English.)
31. Schröder R, Keller E, Flacke S, Schmidt S, Pohl C, Klockgether T, Schlegel U. MRI findings in Hirayama's disease: flexion-induced cervical myelopathy or intrinsic motor neuron disease? J Neurol. 1999;246:1069–74.
32. Hirayama K. Juvenile muscular atrophy of distal upper extremity (Hirayama disease). Intern Med. 2000;39:283–90.
33. Hirayama K, Tokumaru Y. Cervical dural sac and spinal cord in juvenile muscular atrophy of distal upper extremity. Neurology. 2000;54:1922–6.
34. Hirayama K. Juvenile muscular atrophy of distal upper extremity (Hirayama disease): Focal cervical ischemic poliomyelopathy. Neuropathology. 2000;20:S91–4.
35. Mukai E, Sobue I, Muto T, Takahashi A, Goto S. Abnormal radiological findings on juvenile type distal and segmental muscular atrophy of upper extremities. Rinsho Shinkeigaku. 1985;25:620–6. (In Japanese, abstract in English.)
36. Kikuchi S, Tashiro K, Kitagawa M, Iwasaki Y, Abe H. A mechanism of juvenile muscular atrophy localized in hand and forearm (Hirayama disease). Flexion myelopathy with tight dural canal in flexion. Rinsho Shinkeigaku. 1987;27:412–9. (In Japanese, abstract in English.)
37. Tokumaru Y, Hirayama K. Pathomechanism of juvenile muscular atrophy of unilateral upper extremity (Hirayama disease). Extensibility and asymmetry of the cervical posterior dural wall. Rinsho Shinkeigaku. 1994;34:996–1002. (In Japanese, abstract in English.)
38. Kikuchi S, Tashiro K. Juvenile muscular atrophy of distal upper extremity (Hirayama disease). In: Johes HR Jr, DeVivo DC, Darras BT, editors. Neuromuscular Disorders of Infancy, Childhood, and Adolescence: A Clinician's Approach. Philadelphia: Butterworth Heinemann: Elsevier Science; 2003. pp 167–81.
39. Kijima M, Hirayama K, Nakajima Y. Symptomatological and electrophysiological study on cold paresis in juvenile muscular atrophy of distal upper extremity (Hirayama disease). Rinsho Shinkeigaku. 2002;42:841–8. (In Japanese, abstract in English.)
40. Yada K, Tachibana S, Okada K. Spinal cord lesion due to relative imbalance of cervical spine and spinal cord. 1981 Annual Report of Prevention and Treatment for the Congenital Anomalies of the Spine and Spinal Cord. The Ministry of Health and Welfare of Japan:. 1982;110:5. (In Japanese.)
41. Kohno M, Takahashi H, Ide K, Yamakawa K, Saitoh T, Inoue K. Surgical treatment for patient with cervical flexion myelopathy. J Neurosurg. 1999;91:33–42.
42. Tokumaru Y, Hirayama K. A cervical collar therapy for non-progressive juvenile spinal muscular atrophy of the distal upper limb (Hirayama disease). Rinsho Shinkeigaku. 1992;32:1102–6. (In Japanese, abstract in English.)
43. Tokumaru Y, Hirayama K. Cervical collar therapy for juvenile muscular atrophy of distal upper extremity (Hirayama disease): results from 38 cases. Rinsho Shinkeigaku. 2001;41:173–8. (In Japanese, abstract in English.)

Acta Neuropathol (2006) 112: 52–63
DOI 10.1007/s00401-006-0056-x

ORIGINAL PAPER

Hisae Sumi · Seiichi Nagano · Harutoshi Fujimura
Shinsuke Kato · Saburo Sakoda

Inverse correlation between the formation of mitochondria-derived vacuoles and Lewy-body-like hyaline inclusions in G93A superoxide-dismutase-transgenic mice

Received: 31 May 2005 / Revised: 12 February 2006 / Accepted: 12 February 2006 / Published online: 27 April 2006

Abstract In G93A mice, the most popular model of amyotrophic lateral sclerosis (ALS), neuronal Lewy-body-like hyaline inclusions (LBHIs) and mitochondria-derived vacuoles are observed in addition to motor neuron loss. Although LBHIs are thought to be toxic, the significance of the mitochondria-derived vacuoles has not been fully investigated. In this study, the relationship between the formation of these vacuoles and LBHIs was clarified statistically in the lumbar segment from two phyletic lines of G93A mice (G1L, G1H), using immunohistochemical methods. Furthermore, the distributions of vacuoles and LBHIs were examined in the pons including the facial nucleus, where pathological changes occur in ALS patients and G93A mice. Numerous vacuoles 2–3 μm in diameter were detected in the neuropil of the lumbar segment from G1L mice euthanatized approximately 3.5 months prior to the onset of the disease. Most of the vacuoles disappeared, but some became larger as the disease progressed. The number of vacuoles with a diameter exceeding 5 μm began to decrease after disease onset, while that of intra-neuritic LBHIs increased rapidly. There was a strong inverse correlation between the numbers of vacuoles and LBHIs in symptomatic mice ($P<0.01$; G1L, $r=-0.91$; G1H, $r=-0.93$). In the facial nucleus of G1L mice, where the number of motor neurons was significantly reduced, only a few LBHIs were detected along with prominent vacuole formation. In contrast, significantly more LBHIs with little vacuole formation were evident around the facial nucleus in G1L mice. Furthermore, the SOD1 immunoreactivity in vacuoles initially increased and then decreased after disease onset. Taken together, the present findings suggest that the mitochondria-derived vacuoles might prevent the formation of LBHIs by sequestering mutated SOD1 from the cytoplasm.

Keywords Vacuole · Lewy-body-like hyaline inclusion · Mitochondria · Transgenic mice · Amyotrophic lateral sclerosis

H. Sumi (✉) · S. Nagano · H. Fujimura · S. Sakoda
Department of Neurology D-4, Osaka University Graduate School of Medicine, 2-2, Yamadaoka, Suita, 565-0871 Osaka, Japan
E-mail: hasumi@neurol.med.osaka-u.ac.jp
Tel.: +81-6-68793571
Fax: +81-6-68793579

S. Kato
Department of Neuropathology, Institute of Neurological Sciences, Faculty of Medicine,
Tottori University, Yonago, Japan

Introduction

Amyotrophic lateral sclerosis (ALS) is a fatal motor neuron disease whose pathogenesis remains unknown. About 10% of ALS cases are familial and approximately 15–20% of familial ALS patients possess the copper/zinc superoxide dismutase (SOD1) gene mutation [8, 40]. Since transgenic mice or rats carrying the human mutated SOD1 gene (SOD1 mice or rats) develop progressive motor deficits caused by loss of anterior horn cells [3, 12, 16, 32, 39, 56], they have been used by many researchers as a model of ALS. SOD1 mice or rats carrying different mutated SOD1 genes have been reported to show different pathologic features: in G93A mice or rats, many Lewy-body-like hyaline inclusions (LBHIs) and mitochondria-derived vacuoles are observed [6, 7, 32]; in G85R or G86R mice, many LBHIs, but almost no vacuoles, appear long before the onset of the disease [3, 39]; in H46R rats, many LBHIs and very few vacuoles are found [32]; in G37R mice, there is prominent vacuole formation and almost no LBHIs [55, 56]. Although in G85R mice the level of mutant G85R SOD1 protein expressed is only 20% of endogenous SOD1, these mice show very progressive motor deficits [3]. Other SOD1

mice or rats express a mutant protein level approximately 10 times higher than that in murine SOD1 [12, 16, 32, 56]. Several lines of G93A or G37R mice with different levels of mutant protein expression show different pathologic features [6, 7, 56]. Thus, the differences in neuropathology observed among SOD1 mice or rats appear to depend on the character of the mutant protein and its level of expression.

SOD1-positive LBHIs in neurons are neuropathological hallmarks of familial ALS linked with SOD1 mutation [15, 17, 22, 44]. In cell lines transfected with mutated SOD1, aggregations of mutated SOD1 or LBHI-like structures are formed [9, 21, 46]. In SOD1 mice or rats, such aggregates of SOD1 or LBHIs appear before onset of the disease [3, 4]. These aggregates of SOD1 or LBHIs, which are found specifically in the affected spinal cord or brainstem [15, 44, 54], are resistant to strong detergents or reducing agents. Although formation of aggresomes [21] or inclusions such as Lewy bodies in Parkinson's disease might be considered the result of cell-protective responses to various forms of stress [36], aggregation of mutant SOD1 or the formation of LBHIs in SOD1-mutated ALS is reported to have a toxic effect [4, 5, 23] due to sequestration of the components that are essential for maintaining cell functions [24, 25], induction of repetitive misfolding and reduction of chaperone function [2], or reduction of the activity of the proteasome integral for protein turnover [20, 21, 53].

The most important function of mitochondria in cells is the production of ATP, which is indispensable for sustaining life. Cytochrome *c* oxidase (CCO), which is located in the inner membrane of the mitochondrion and, in mammals, is composed of 13 different subunits, participates in electron transport within mitochondria [30]. Cytochrome *c* (cyt *c*) is oxidised by CCO through electron transport in the intermembrane space of the mitochondrion [38]. The large amount of energy required for action potentials in neurons depends on the ATP produced by mitochondria through electron transport. In G93A mice, the most widely used animal model of ALS, one of the very early pathologic features is the appearance of vacuoles followed by that of abnormal mitochondria [6, 14, 28, 42, 43], suggesting that the vacuoles are derived from mitochondria [14, 28].

The formation of LBHIs has been thought to have toxic effects, but the significance of the vacuoles remains unclear. Since the vacuoles appear far earlier than the LBHIs, an investigation of vacuoles would be important for clarifying the pathogenesis of the disease in G93A mice. In the study presented here, we carried out a quantitative examination of the vacuoles using an immunohistochemical method and analyzed the relationship between the vacuoles and the formation of LBHIs in the lumbar segment or facial nucleus of G93A mice in order to clarify the significance of mitochondria-derived vacuoles.

Materials and methods

Animals

Transgenic mice expressing the G93A mutated human SOD1 gene at a low (B6SJL-TgN[SOD1-G93A]1Gur^{dl}, G1L) or high (B6SJL-TgN[SOD1-G93A]1Gur, G1H) level were obtained from the Jackson Laboratory (Bar Harbor, ME, USA). These mice were bred and maintained as hemizygotes by mating with wild-type B6SJL mice. Non-transgenic littermates were used as controls. All animals were genotyped using polymerase chain reaction amplification of the tail DNAs under conditions that have been described previously [33]. All animals were handled in accordance with the Guidelines for the Care and Use of Laboratory Animals at Osaka University Graduate School of Medicine. We evaluated the animals clinically, examining their hindlimb extension when they were suspended in the air by the tail [1, 33, 34, 49].

Tissue preparation

We examined control (260 ± 6 days old), G1L, and G1H mice ($n = 3$ in each group). G1L mice were euthanatized at the age of 90, 140 (the asymptomatic stage), 180 (the presymtomatic stage), 230 days (the symptomatic stage) or at the end stage when they could hardly move or drink water because of severe paralysis (259 ± 6 days old, the moribund state). G1H mice were euthanatized at the age of 66 (the asymptomatic stage), 100 (the early symptomatic stage), or 115 days (the late symptomatic stage). They were deeply anesthetized with sodium pentobarbital, and perfused with phosphate-buffered saline (PBS, pH 7.4) followed by 4% paraformaldehyde. The brainstem and spinal cord were removed, immersed in the same fixative overnight at 4°C, and then cryoprotected. Ten-micrometer-thick frozen sections were prepared and stained with hematoxylin and eosin (HE). Small pieces of lumbar segments were fixed with 2.5% glutaraldehyde in 0.1 M PB (pH 7.4) for 2 h at 4°C, followed by 1% osmium tetroxide in 0.1 M PB at 4°C, dehydrated in an ethanol series and embedded in Epon; LUVEAK-812 (glycerol triglycidyl ether, Nakarai Tesque, Kyoto, Japan)/LUVEAK-DDSA (dodecylsuccinic anhydride, Nakarai Tesque)/LUVEAK-MNA (methylnadic anhydride, Nakarai Tesque)/LUVEAK-DMP-30 (2,4,6-Tris (dimethylaminomethyl) phenol, Nakarai Tesque). Transverse sections 1 μm thick were stained with toluidine blue.

Immunohistochemical analysis of vacuoles in lumbar segment and brainstem

For immunohistochemical evaluations, frozen or deparaffinized sections were incubated for 30 min with

0.3% H_2O_2 to quench endogenous peroxidase activity and then washed with PBS. Normal goat serum was used as a blocking reagent. Mouse monoclonal antibodies against cyt *c* (1:100 in 1% PBS containing bovine serum albumin, clone 6H2.B4, BD PharMingen, CA, USA), CCO subunit I (1:400 clone 1D6, Molecular Probes Inc, OR, USA), human SOD1 (0.5 μg/ml, clone 1G2, MBL, Aichi, Japan) or GFAP (ready to use, DAKO, Glostrup, Denmark) were used as primary antibodies. Tissue sections were incubated with each primary antibody for 18 h at 4°C. The avidin–biotin–immunoperoxidase complex (ABC) method was employed according to the manufacturer's instructions to detect each bound antibody using the appropriate Vectastain ABC kits (Vector Laboratories, Burlingame, CA, USA). 3,3′-Diaminobenzidine tetrahydrochloride (DAKO, Glostrup, Denmark) was used as the final chromogen. Hematoxylin was used to counterstain cell nuclei. In control experiments, primary antibodies were omitted from the incubation medium.

Quantitative evaluation of motor neurons, LBHIs and cyt *c*-positive vacuoles in the lumbar segment

To estimate the number of neurons in the gray matter (VII, VIII, IX Rexed areas) showing clear nucleoli and cell bodies with a diameter greater than 25 μm [26, 28, 48], presumed to be alpha motoneurons [10, 30, 31], video images of the anterior horns were obtained with a digital camera (KEYENCE VB-7010, KEYENCE, Osaka, Japan) attached to a light microscope (ECLIPSE E800, Nikon, Tokyo, Japan) for each section, and the areas of motor neurons showing clear nucleoli and cell bodies were measured using image analysis software (VH-H1A5, KEYENCE). The number of neurons with a diameter greater than 25 μm were counted in HE-stained sections. LBHIs with a halo and core and cyt-*c*-positive vacuoles in the gray matter were also counted (×100 objective). LBHIs were also confirmed using antibodies against human SOD1 and GFAP. Since the vacuoles are contained exclusively in neuronal processes [19, 43], and not in astrocytes, only neuronal LBHIs were counted to examine the relationship between the vacuoles and LBHIs in neurons. LBHIs in cells possessing glial nuclei were omitted. To establish how the size and number of vacuoles in the lumbar segments of G1L mice changes chronologically over the clinical course of the disease, vacuoles were divided according to size into small (< 5 μm) or large (> 5 μm). Every fifth section (40 μm interval) was obtained, and three sections from each mouse were used to obtain the total number of neurons, LBHIs or vacuoles. The quantitative evaluation was analyzed statistically. Moreover, the relationship between the number of vacuoles and LBHIs was estimated in each symptomatic mouse (G1L, 230 days and the moribund state 259 ± 6 days; G1H, 100 and 115 days).

Quantitative analysis of LBHIs in the pons including the facial nucleus

For histological analyses of the facial nucleus (nVII), we examined non-transgenic littermates ($n=3$, 264 ± 7 days) and G1L mice in the moribund state ($n=7$, 258 ± 7 days). Each carefully hemisected brainstem was embedded in paraffin and sectioned transversely. The pons including the nVII was identified in these sections, with reference to the mouse brain atlas of Paxinos and Franklin [37]. Six-micrometer-thick paraffin sections were prepared and stained with HE. In the nVII, large neurons with clear nucleoli and cell bodies were counted. LBHIs located in three subregions of the pons (vacuole-rich area = intra-nVII, the border zone, and vacuole-poor area, as delineated in Fig. 1) were also counted (×40 objective). To estimate the number of LBHIs per unit area in each subregion, video images of the pons were obtained with a digital camera (KEYENCE VB-7010, KEYENCE, Osaka, Japan) attached to a light microscope (ECLIPSE E800, Nikon, Tokyo, Japan) for each section, and the areas of three subregions were measured using image analysis software (VH-H1A5, KEYENCE). Every fifth section (at 24-μm intervals)

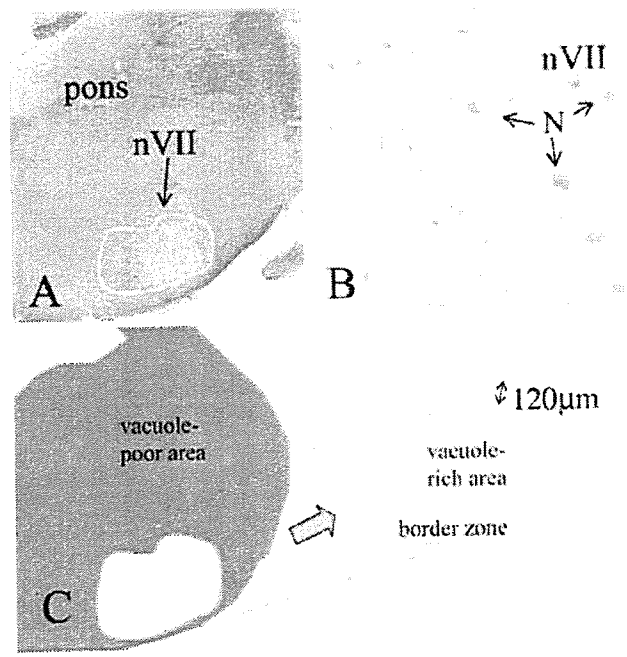

Fig. 1 Schematic diagram of the three subregions in the pons; vacuole-rich area (= intra-nVII), the border zone and vacuole-poor area. The boundary of massive vacuole formation limited to the facial nucleus (nVII) is shown at low (**a**) and high (**b**) magnification as a *yellow line*, using actual microscopic fields digitized for illustrative purposes. The definition of the vacuole-rich area (= intra-nVII), border zone and vacuole-poor area is as follows: vacuole-rich area (*light blue*) corresponds to the inner area outlined in *yellow*; the border zone (*white*) corresponds to the surrounding area outlined in *yellow and green*, 120 μm exterior to the *yellow line*; the vacuole-poor area (*pink*) corresponds to the outer area of the pons excluding the other two regions. *N* neuron

was obtained, and three sections from each mouse were used to obtain the total number of neurons and the density of LBHIs. The number of motor neurons and the density of LBHIs were analyzed statistically. All quantitative investigations were performed independently by three neuropathologists (HS, HF, SK).

Statistics

Data are expressed as the mean ± standard error of the mean (SEM). All statistical analyses of histopathological data were carried out using the Statview for Macintosh software package (Ver5.0, SAS Institute Inc, CA, USA). A nonparametric test, Mann–Whitney *U* test, was used to analyze the number of neurons, LBHIs and vacuoles in the lumbar segment or the number of neurons and the density of LBHIs in the pons. The relationship between the number of LBHIs and vacuoles in the lumbar segment was estimated by regression analysis.

Results

Morphological changes of vacuoles in the lumbar segment of G1L or G1H mice

Many tiny vacuoles 2–3 μm in diameter were found in neurites mainly at the edge of the anterior horn in G1L mice at 90 days (Fig. 2a). Some of the vacuoles were hardly distinguishable from capillary vessels. At 140 days, larger but fewer vacuoles than those at 90 days were observed in the same area (Fig. 2b). Vacuoles were also scattered diffusely in the anterior horn. At 180 days, round vacuoles larger than those at 140 days (Fig. 2c) were frequently found throughout the gray matter. At the later stages in G1L mice, the large vacuoles appeared slightly deformed and were reduced in number (Fig. 2d). Many LBHIs were scattered in the gray matter. In G1H mice, more prominent vacuole formation was observed (Fig. 4a, d) than that in G1L mice. The vacuoles became larger and their number was reduced by 115 days (Fig. 4d) in comparison with those at 100 days (Fig. 4a). Although at 100 days the vacuoles were observed mainly in the anterior horn, by 115 days their distribution had also extended to the whole of the gray matter.

Immunohistochemical analyses of vacuoles in the lumbar segment of G1L mice

As a negative control, sections were incubated without the primary antibody; this resulted in no staining in the lumbar segments of normal and G93A low-copy transgenic mice (G1L mice). As expected, the cytoplasm of motor neurons was clearly stained for cyt *c* or CCO in the lumbar segment of normal mice (Fig. 3a, b). The staining pattern with the two antibodies was similar, showing a fine granular pattern. The neuropil was also weakly stained for these antibodies. The immunohistochemical analysis revealed many tiny vacuoles, strongly positive for cyt *c* at the edge of the anterior horn in G1L mice (90 days; Fig. 3c–e). Some vacuoles were scattered in the neuropil of the anterior horn. Axons were lined with tiny vacuoles that appeared to be attached together. The rim of the vacuoles in the neuropil was stained for cyt *c* (Fig. 3d, e). The structures lying interior to the vacuolar rim were CCO-positive, although the rim itself was CCO-negative. At 140 days, the number of vacuoles was lower than that at 90 days. In contrast, large vacuoles (> 5 μm), which were never seen at 90 days, were frequently observed at the edge of the anterior horn (Fig. 3f). The cyt *c* immunoreactivity was reduced within the rim of these large vacuoles (Fig. 3f, g). Small vacuoles (< 5 μm) did

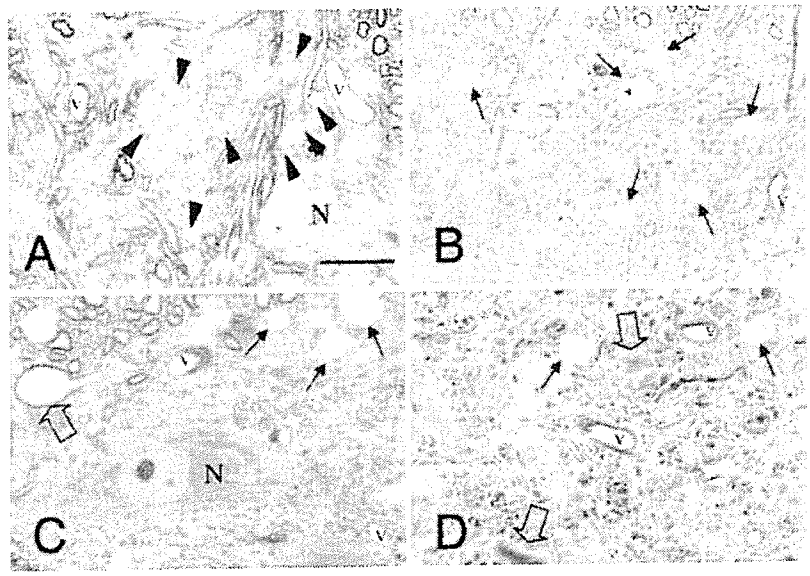

Fig. 2 Morphological changes in vacuoles in the anterior horn of G1L mice at different stages. (Epon sections, toluidine blue, **a** 90 days, **b** 140 days, **c** 180 days, **d** end stage). **a** Many small vacuoles (< 5 μm, *arrow heads*) are evident at the edge of the anterior horn. **b** The number of vacuoles has decreased. Vacuoles (*arrows*) at the edge of the anterior horn have become larger. **c** The number of vacuoles (*arrows*) is smaller than in **b**. Note the large vacuoles in neurites including axons (*clear arrow*). **d** Only a few vacuoles (*arrows*) are evident. LBHIs (*clear arrow*) appear in the anterior horn. *N* neuron; *V* vessels. Scale bar **a** (also for **b–d**) 20 μm

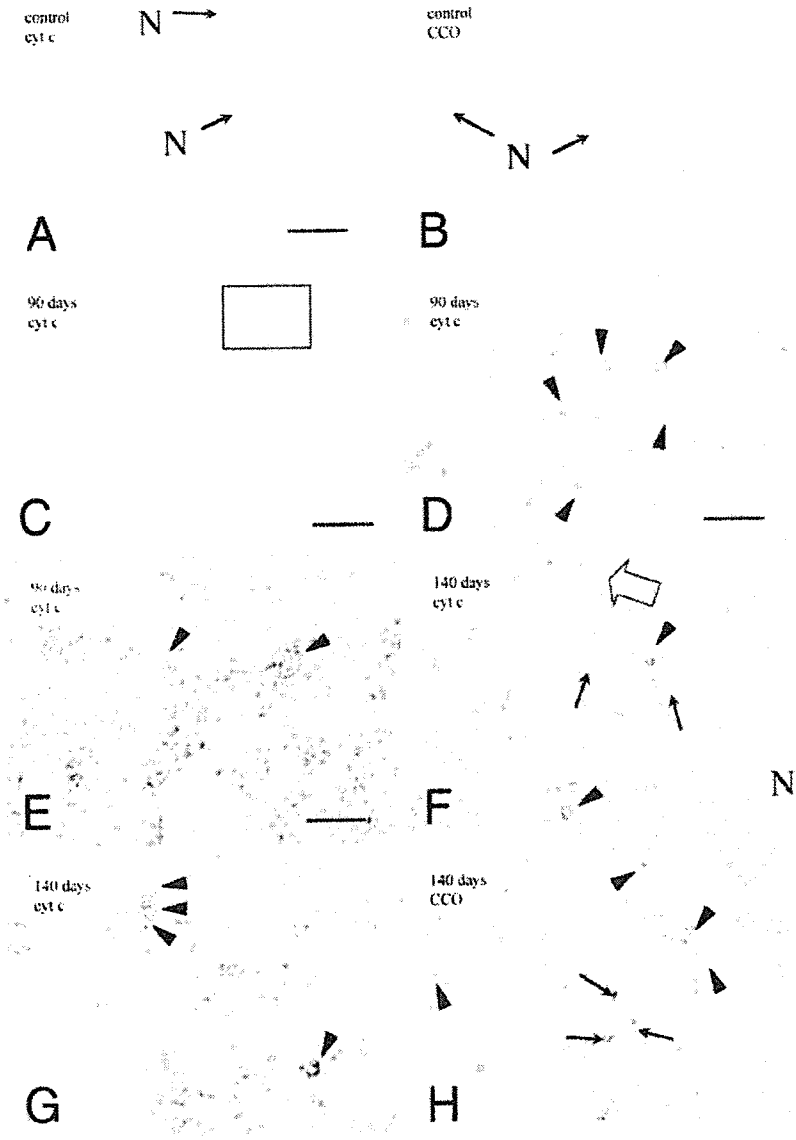

Fig. 3 Immunohistochemistry of vacuoles in the anterior horn of G1L mice (**a**, **b** normal control, **c–l** G1L mice; **a**, **b** 263 days, **c–e** 90 days, **f–h** 140 days, **i** 180 days, **j**, **k** 230 days, **l** end stage; **a**, **c–g**, **j**, **l** cyt *c*, **b**, **h**, **i**, **k** CCO). **a** A fine granular staining pattern is evident in the cytoplasm of motor neurons (*N*, *arrows*). The neuropil is also weakly stained. **b** Motor neurons (*N*, *arrows*) show well-defined cytoplasmic staining for CCO. Diffusely scattered fine dots can be seen in the neuropil. **c–e** Tiny, densely immunolabeled vacuoles within the rim (*arrow heads*) are prominent at the edge of the anterior horn. **d** is a high magnification view of **c**. **e** is a high magnification view of **d**. **f** The number of vacuoles is lower than in **d**. Large vacuoles (> 5 μm, *arrows*), which were never seen in **d**. The immunoreactivity for cyt *c* is reduced within the rim of large vacuoles (*arrows*) compared to that of small vacuoles (< 5 μm, *arrow heads*). In axons, tiny vacuoles are tightly packed to form a columnar shape (*clear arrow*). **g** is a high magnification view of **f**. **h** Abnormal structures lying interior to the rim of vacuoles (*arrows*, *arrow heads*) are strongly positive for CCO. Irregular CCO-positive dots (*arrow heads*) are scattered in the neuropil. **i** Large CCO-positive complexes lying interior to the rim of large vacuoles. **j** The number of vacuoles (*arrow*, *arrow head*) is lower than that in **i**. Cyt-*c*-positive small vacuoles (*arrow head*) are seen only rarely. **k** CCO-positive complexes (*arrows*) lying interior to the vacuolar rim have become atrophic in comparison with those in **i**. **l** Small vacuoles are not evident. Some large vacuoles (*arrows*) remain. *N* neurons; *V* vessels. Scale bars: **a** (also for **b**)50 μm, **c** 100 μm, **d** (also for **f**, **h–l**) 20 μm, and **e** (also for **g**) 10 μm

not fuse to form a large vacuole. Some small and large vacuoles were found in the dorsal horn. Each vacuole had CCO-positive structures lying interior to the rim (Fig. 3h). At 180 days, there was a reduction in the number of small vacuoles (< 5 μm), and many large vacuoles (> 5 μm) were found scattered not only at the edge of the anterior horn, but also throughout the neuropil. These vacuoles had highly CCO-positive structures lying interior to the rim (Fig. 3i). At later stages, the tiny, strongly cyt *c*-positive vacuoles were

Fig. 3 (Contd.)

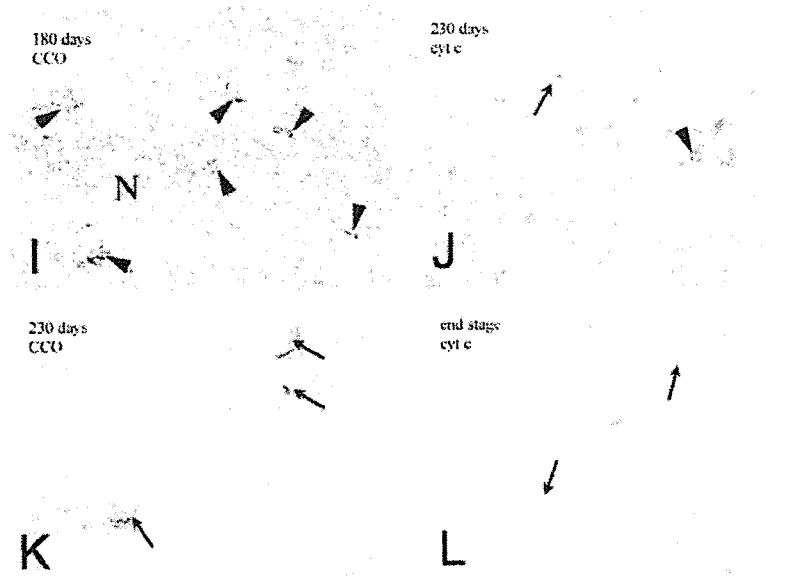

seen only rarely (Fig. 3j, l), and some large vacuoles were observed scattered throughout the neuropil. The CCO-positive structures lying interior to the vacuole rim became atrophic (Fig. 3k), especially in moribund mice. Cyt *c*-positive vacuoles were never seen in the soma of neurons from G1L mice.

Immunohistochemical analyses of vacuoles in the lumbar segment of G1H mice

In symptomatic G1H mice (100 and 115 days), prominent vacuole formation was observed (Fig. 4b, c, e, f). The vacuolar rims were cyt-*c*-positive and there were

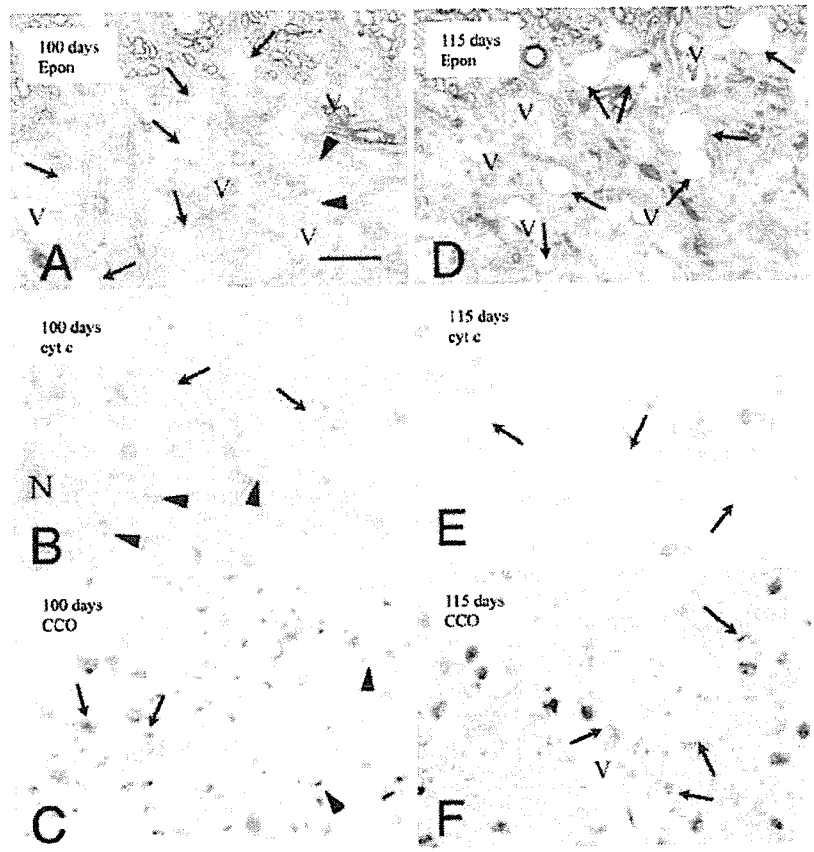

Fig. 4 More prominent vacuole formation with similar immunostaining patterns for cyt *c* and CCO in the anterior horn of G1H mice (**a–c**; 100 days, **b–f**; 115 days, **a**, **d**; Epon sections, toluidine blue, **b**, **e**; cyt *c*, **c**, **f**; CCO). **a** Abundant small (< 5 μm, *arrow heads*) or large (> 5 μm, *arrows*) vacuoles are present in neurites. **b** Cyt-*c*-positive staining in the rim of small (*arrow heads*) and large (*arrows*) vacuoles. The immunoreactivity of the large vacuoles (*arrows*) is reduced, as in G1L mice. **c** CCO-positive structures are evident in small (*arrow heads*) or large vacuoles (*arrows*). **d** The number of vacuoles is reduced. Larger vacuoles than those in **a** are frequently evident. **e** Large vacuoles about 15–20 μm in diameter (*arrows*) are observed more frequently than in the G1L lumbar segment. **f** Somewhat atrophic CCO-positive structures (*arrows*) lying interior to the rim of large vacuoles. *N* neurons; *V* vessels. Scale bar, **a** (also for **b–f**) 20 μm

CCO-positive structures lying interior to them, as observed in G1L mice. Cyt *c* immunoreactivity was reduced in the large vacuoles (Fig. 4b, e). The structures lying interior to the vacuolar rim, evident at 100 days (Fig. 4c), became rather atrophic by 115 days (Fig. 4f). At 100 days, the ratio of the number of large vacuoles (> 5 μm) to the total number of vacuoles was more than 50% (Fig. 4b); this figure had reached almost 90–100% by 115 days (Fig. 4e). The vacuoles in G1H mice tended to be larger than those in G1L mice.

Quantitative analysis of the vacuoles, LBHIs and motor neurons in the lumbar segment of G1L and G1H mice

Figure 5 shows the number of small (< 5 μm) and large (> 5 μm) vacuoles, and LBHIs and motor neurons (> 25 μm) in the lumbar segment during the clinical course of the disease in G1L mice. Numerous small vacuoles were already evident at 90 days, and their number decreased as the disease progressed (Fig. 5a, Table 1, $P < 0.05$). The number of large vacuoles, which appeared at around 140 days, were increased significantly by 180 days but then decreased significantly by 230 days (Fig. 5a, Table 1, $P < 0.05$). The ratio of the number of large vacuoles to the total number of vacuoles was 10–20% at 140 and 180 days, and ~50% in moribund mice (Fig. 5a). In G1H mice, the total number of vacuoles showed a tendency to decrease, but not to a significant degree (Table 1, $P = 0.1266$). The number of neurons declined significantly after 180 days in G1L mice, and after 66 days in G1H mice (Table 1, $P < 0.05$). LBHIs were restricted to the anterior horn at 180 and 100 days in G1L and G1H mice, respectively, becoming more widespread at the later stages. The number of LBHIs increased significantly in G1L or G1H mice as the disease progressed (Fig. 5b, Table 1, $P < 0.05$). Most of the LBHIs were intra-neuritic.

Correlation between the numbers of vacuoles and LBHIs in symptomatic G1L and G1H mice

Figure 6 shows the correlation between the numbers of vacuoles and LBHIs observed in symptomatic G1L (230 days and in the moribund state) and G1H (100 and 115 days) mice. The number of vacuoles in G1H mice was greater than in G1L mice. Regression analysis revealed a statistically significant inverse correlation between the numbers of vacuoles and LBHIs in both G1L ($r = -0.91$, $P < 0.01$) and G1H ($r = -0.93$, $P < 0.01$) mice.

Quantitative analysis of LBHIs in the nVII and the differential localization of LBHIs and vacuoles

HE staining revealed atrophic motor neurons with prominent vacuole formation in the nVII of moribund G1L mice. Most of the vacuoles in the nVII (Fig. 7b)

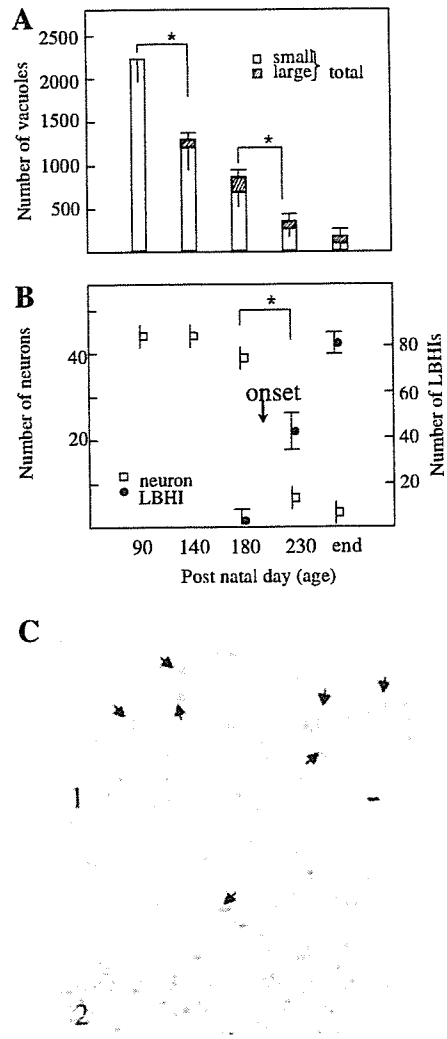

Fig. 5 Time course of changes in the number of vacuoles (**a**), LBHIs and motor neurons (**b**) in the anterior horn of G1L mice. **a** Numerous small vacuoles are evident at 90 days. The number of small vacuoles decreases significantly with disease progression (*$P < 0.05$). The large vacuoles are present from 140 days, and their number then increases significantly by 180 days, followed by a significant decrease by 230 days. **b** The number of neurons (> 25 μm) declines significantly after 180 days (*$P < 0.05$) and, conversely, the number of LBHIs increases significantly after 180 days (*$P < 0.05$). Data are presented as mean ± SEM ($n = 3$ for each group). **c** Representative hematoxylin and eosin (HE) staining of the anterior horn in control (**1**) and G1L mice at the end stage (**2**). The number of neurons (> 25 μm, *arrows*) is reduced in (**2**). Scale bar **c** 25 μm

were larger than those observed in the lumbar segment. The number of motor neurons in the nVII was significantly reduced (Table 2, $P < 0.05$), and LBHIs were found only rarely in the vacuole-rich area (= intra-nVII). In marked contrast, LBHIs were found frequently in the border zone (see Materials and methods), but there were very few vacuoles (Fig. 7c). Most of the vacuoles were located in the neuropil, and not in the soma of neurons (Fig. 7d). Most of the LBHIs were also

Table 1 Number of anterior horn cells, vacuoles and LBHIs in the lumbar segments of G1L and G1H mice (values are given as mean ± SEM)

	G1L						G1H		
	90 days	140 days	180 days	230 days	259 ± 6 days	Non-transgenic (260 ± 6 days)	66 days	100 days	115 days
Anterior horn cells	43 ± 1	43 ± 2	39 ± 2	8 ± 3[b]	4 ± 1[b]	41 ± 1	41 ± 2	31 ± 3[c]	14 ± 3[d]
Vacuoles (total)	2,243 ± 151	1,307 ± 188[a]	842 ± 139[a]	314 ± 42[b]	198 ± 115[b]	0	ND	1,832 ± 259	1,078 ± 201
LBHIs	0	0	4 ± 3	44 ± 18[b]	83 ± 6[b]	0	0	11 ± 3	30 ± 6[d]

G1L Mutant SOD1 (G93A) low-copy mouse; *G1H* mutant SOD1 (G93A) high-copy mouse; *SEM* standard error of the mean; *LBHI* Lewy-body-like hyaline inclusion; *ND* not determined
[a] $P < 0.05$ compared with G1L mice at 90 days; [b] $P < 0.05$ compared with G1L mice at 180 days; [c] $P < 0.05$ compared with G1H mice at 66 days; [d] $P < 0.05$ compared with G1H mice at 100 days

intra-neuritic. The LBHIs in the border zone were larger than those in the vacuole-rich area (=intra-nVII). Quantitative analysis of data from the three subregions of the pons demonstrated a preferential localization of LBHIs to the border zone, the area surrounding the nVII (Table 2, $P < 0.01$).

Immunohistochemical analysis of vacuoles in the facial nucleus of G1L mice

Immunohistochemical analysis of vacuoles in the facial nucleus (nVII) showed that abundant tiny cyt-*c*-positive vacuoles appeared at the edge of the nVII at an early stage (Fig. 8a), similar to those in the lumbar segments. As the disease progressed, the vacuoles became larger (Fig. 8b–f) and were distributed throughout the nVII. Thereafter, although their number decreased progressively, a considerable amount of large vacuoles remained in the nVII even at the end stage (Figs. 7b, 8f). The immunoreactivity for cyt-*c* was weaker in the larger vacuoles than in the tiny vacuoles (Fig. 8b). Immunohistochemical staining for mutant SOD1 showed that the rim of the vacuoles was stained at an early stage (Fig. 8c, d). The SOD1 immunoreactivity of the rim increased at 140 days (Fig. 8d). By 180 days, not only the rim, but also the core of the vacuoles became SOD1-positive (Fig. 8e). At the end stage, the SOD1-positive structures inside the vacuoles decreased. Most of the vacuoles, except for those present in axons, showed weak immunoreactivity for SOD1 in their rim. Vacuoles that were almost SOD1-negative were frequently observed (Fig. 8f).

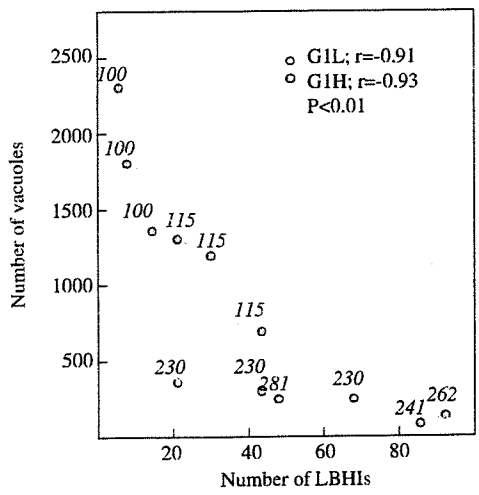

Fig. 6 Inverse correlation between the numbers of mitochondria-derived vacuoles and LBHIs. A statistically significant inverse correlation was observed between the numbers of LBHIs and vacuoles in both G1L (*green*) and G1H (*orange*) mice. Numbers shown in *italics* represent the age of the G93A mice at perfusion

Discussion

In the G93A mouse, the most commonly studied model of ALS, the characteristic neuropathological features are LBHIs and vacuoles [6, 7]. Although scarcely found in FALS patients associated with SOD1 gene mutation [41], it has been considered important to investigate vacuoles [18, 19, 28, 42, 43] because the model mice overexpressing the mutant SOD1 protein could provide clues for understanding the characteristics of mutant SOD1. Also, since evaluation of LBHIs, which are the hallmarks of FALS linked with SOD1 gene mutation, is indispensable for pathological analysis, it is necessary to clarify the factors that can influence their formation.

In control mice, the cytoplasm of the motor neurons showed granular staining with antibodies against subunit I of CCO, a component of the mitochondrion-specific enzyme that is localized in the inner membrane [50], and against cyt *c*, a mediator of CCO that is localized in the intermembrane space [38]. The staining with these antibodies in the motor neurons of control mice corresponds to the localization of mitochondria [11, 19]. In G93A mice, the rims of vacuoles were cyt-*c*-positive and CCO-negative, and the structures lying interior to the vacuolar rim were CCO-positive and cyt-*c*-negative. The latter structures are probably non-functional mitochondrial membrane remnants [14, 28, 43]. Since cyt *c* is released into the cytosol from the permeability transition pores of injured mitochondria [11, 27, 29, 45, 47, 57, 58], the presence of a cyt-*c*-positive

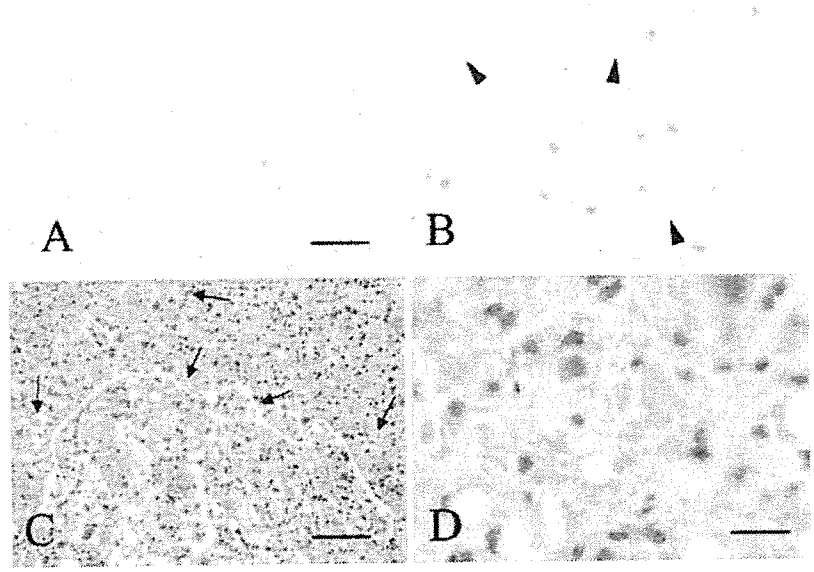

Fig. 7 Representative hematoxylin and eosin staining in the nVII of control (**a**; 261 days) and G1L (**b–d**; end stage) mice. **a**, **b** The number of motor neurons in the G1L nVII is reduced, and all of the residual neurons are atrophic in G1L mice as compared with the controls. Note the prominent vacuolization (*arrow heads*) and lack of LBHIs inside the G1L nVII. **c** Many LBHIs are present (*arrows*, *white arrow*) in the area surrounding the nVII. The *yellow line* delineates the vacuole-rich area (=intra-nVII). **d** A large LBHI (*white arrow*), more than 10 μm in diameter, is located in a neurite, and not in the soma. Scale bar **a** (also for **b**) 50 μm, **c** 100 μm, and **d** 20 μm

rim might imply that cyt *c* is released from the intermembrane space of injured mitochondria into vacuoles to accumulate along the vacuolar rim. Since both small (< 5 μm) and large (> 5 μm) vacuoles in the neuropil exhibited the same immunostaining patterns for cyt *c* and CCO, and since small vacuoles did not appear to fuse to form large ones, it is thought that the small vacuoles grow to become the large vacuoles [14].

According to a previous report, the appearance of vacuoles in the lumbar segments might be related to the onset, rather than progression of the disease, since the number of vacuoles was found to be maximal at disease onset, and declined thereafter [28]. Using antibodies against mitochondrial components, we have shown here that numerous tiny vacuoles, which are distinguishable from cyt-*c*-negative capillary blood vessels, appear in the neuropil approximately 3.5 months before disease onset [14, 19]. In G1L mice, the number of vacuoles in both the lumbar segment and brainstem decreased progressively thereafter, irrespective of disease onset. In contrast with the findings of the previous study [28], therefore, we have found that the presence of these vacuoles appears to be unrelated to disease onset. Although the number of large vacuoles (> 5 μm) increased until disease onset and decreased thereafter, they appeared to be unrelated to disease onset because the degree of neuron loss in the nVII, exhibiting prominent large vacuoles, was much less marked than in the lumbar segment. If the presence of large vacuoles had been related to disease onset, which is determined by neuron loss, then the degree of neuronal loss in the nVII would have been more severe.

In the lumbar segment, intra-neuritic LBHIs appeared just before disease onset and increased rapidly [55] with the progressive reduction in the number of vacuoles in neurites [28, 42, 43]. Although the number of vacuoles was greater in G1H mice than in G1L mice, there was a statistically significant inverse correlation between the number of vacuoles and LBHIs in symptomatic G1L and G1H mice. In the G1L brainstem with prominent vacuole formation, the number of motor neurons was significantly reduced, in agreement with previous reports [13, 35], but only a few LBHIs were found even at the end stage. A notable observation was the presence of many intra-neuritic LBHIs in the border zone where there were few vacuoles. As LBHI formation is known to occur in affected neurons [15, 44, 54], the LBHIs around the nVII would be contained within the neurites of motor neurons in that area. Therefore, there was an inverse correlation between these two neuro-

Table 2 Number of motor neurons and density of LBHIs in the pons divided into three subregions; vacuole-rich area (=intra-nVII), the border zone and vacuole-poor area (values are given as mean ± SEM)

	Age (days)	Number of motor neurons	Density of LBHIs		
			Vacuole-rich area	Border zone	Vacuole-poor area
G1L	258 ± 7	163 ± 8[a]	1.6 ± 0.5[b]	22 ± 8	1.8 ± 0.7[b]
Non-transgenic	264 ± 7	242 ± 3	0	0	0

nVII facial nucleus; *G1L* mutant SOD1 (G93A) low-copy mouse; *SEM* standard error of the mean; *LBHI* Lewy-body-like hyaline inclusion

The density of LBHIs is the number of LBHIs per 1 mm^2 area

[a] $P < 0.05$ compared with non-transgenic mice; [b] $P < 0.01$ compared with border zone

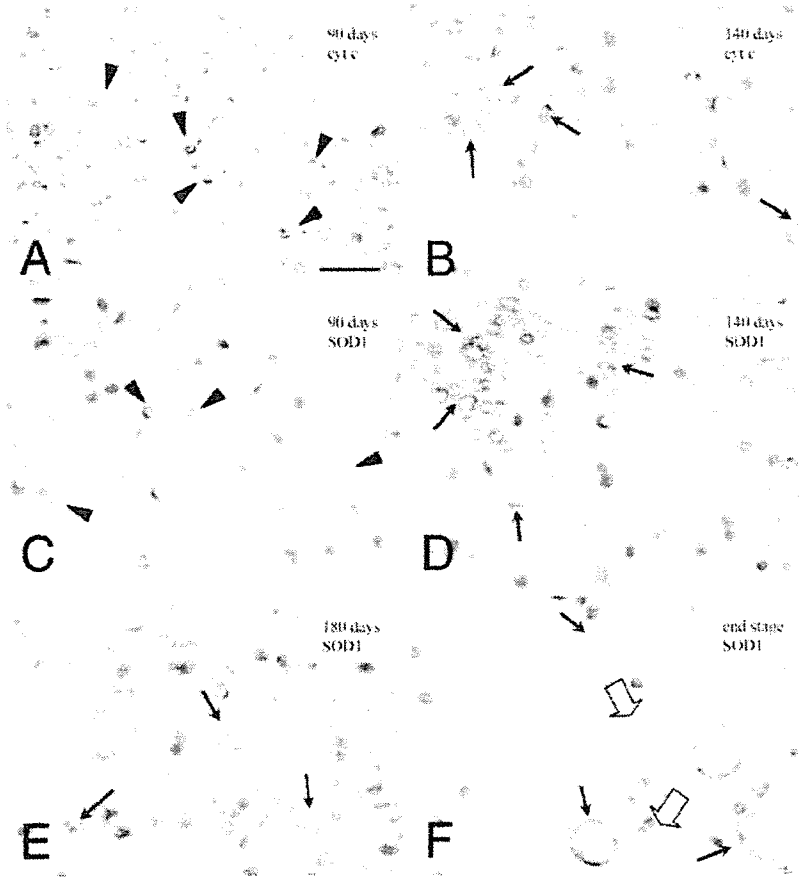

Fig. 8 Immunohistochemical analysis of vacuoles in the nVII of G1L mice (**a**, **c**; 90 days, **b**, **d**; 140 days, **e**; 180 days, **f**; end stage, **a**, **b**; cyt-*c*, **c**–**f**; SOD1). **a** Many tiny cyt-*c*-positive vacuoles (*arrow heads*) are evident. **b** Larger vacuoles (*arrows*) appear, showing lower immunoreactivity than in **a**. **c** Tiny vacuoles (*arrow heads*) are SOD1-positive. **d** SOD1 immunoreactivity becomes stronger at the rim of larger vacuoles (*arrows*) than that of tiny vacuoles observed in **c**. **e** SOD1-positivity is evident not only at the rim, but also the core of the vacuoles (*arrows*). The immunoreactivity has become stronger than that in **d**. **f** Only a few large vacuoles (*arrows*, *clear arrows*) remain. The SOD1 immunoreactivity of vacuoles has become weaker than that in **e**. Some of the vacuoles (*clear arrows*) are almost immunonegative. Scale bar **a** (also for **b**–**f**) 20 μm

pathological changes in both the lumbar segment and the nVII.

Immunohistochemistry using anti-SOD1 antibody revealed that mutant SOD1 accumulated in the rim of tiny vacuoles at an early stage, and was increased in both the rim and the core of the vacuoles [19, 43] until onset. After onset, the intensity of SOD1 immunostaining decreased in both the rim and the core, and SOD1-negative large vacuoles were frequently observed. Since the amount of mutant SOD1 protein increases with age [19, 51], the increased SOD1 immunoreactivity in vacuoles would suggest that more mutant SOD1 was retained in them before onset. The fact that the SOD1 immunoreactivity in vacuoles decreased after onset suggests that vacuoles would not be able to sequester mutant SOD1, despite its higher level of expression in neurons. It is possible that only well-functioning vacuoles at the early stage might be able to retain mutant SOD1. Since mutant SOD1 does not disappear, even when it leaks from vacuoles after onset, it would still remain in the cell [52]. Mutant SOD1 that increased outside vacuoles but remained within the cell would be related to the formation of LBHIs, followed by aggregation of mutant SOD1 in the cell.

In a study using electron and immunofluorescence microscopy, Higgins et al. have reported that the vacuoles originate through expansion of the mitochondrial intermembrane space and extension of the outer mitochondrial membrane and lack lysosomal signals [14]. This suggests that the vacuoles would be produced by a nonautophagic, but still uncharacterized and unique mechanism. In this study, we found a negative correlation between the mitochondria-derived vacuoles and LBHIs, although this does not necessarily mean that the former prevents the latter. However, considering the results of SOD1 immunostaining, it is not unlikely that the mitochondria-derived vacuoles might prevent the formation of LBHIs by sequestering mutated SOD1 from the cytoplasm.

Acknowledgment This study was supported in part by a Health and Labour Sciences Research Grant, Research on Measures for Incurable Disease, Ministry on Health, Labour and Welfare of Japan.

References

1. Barneoud P, Lolivier J, Sanger DJ, Scatton B, Moser P (1997) Quantitative motor assessment in FALS mice: a longitudinal study. Neuroreport 8:2861–2865
2. Bruening W, Roy J, Giasson B, Figlewicz DA, Mushynski WE, Durham HD (1999) Up-regulation of protein chaperones preserves viability of cells expressing toxic Cu/Zn-superoxide dismutase mutants associated with amyotrophic lateral sclerosis. J Neurochem 72:693–699

3. Brujin LI, Becher MW, Lee MK, Anderson KL, Jenkins NA, Copeland NG, Sisodia SS, Rothstein JD, Borchelt DR, Price DL, Cleveland DW (1997) ALS-linked SOD1 mutant G85R mediates damage to astrocytes and promotes rapidly progressive disease with SOD1-containing inclusions. Neuron 18:327–338
4. Brujin LI, Houseweart MK, Kato S, Anderson KL, Anderson SD, Ohama E, Reaume AG, Scott RW, Cleveland DW (1998) Aggregation and motor neuron toxicity of an ALS-linked SOD1 mutant independent from wild-type SOD1. Science 281:1851–1854
5. Cleveland DW, Liu J (2000) Oxidation versus aggregation—how do SOD1 mutants cause ALS? Nat Med 6(12):1320–1321
6. Dal Canto MC, Gurney ME (1994) Development of central nervous system pathology in a murine transgenic model of human amyotrophic lateral sclerosis. Am J Pathol 145:1271–1279
7. Dal Canto MC, Gurney ME (1997) A low expressor line of transgenic mice carrying a mutant human Cu, Zn superoxide dismutase (SOD1) gene develops pathological changes that most closely resemble those in human amyotrophic lateral sclerosis. Acta Neuropathol 93:537–550
8. Deng H-X, Hentati A, tainer JA, Iqbal Z, Cayabyab A, Hung WY, Getsoff ED, Hu P, Herzfeldt B, Roos RP, Warner C, Deng G, Soriano E, Smyth C, Parge HE, Ahmed A, Roses AD, Hallwell RA, Pericak-Vance MA, Siddique T (1993) Amyotrophic lateral sclerosis and structural defects in Cu/Zn superoxide dismutase. Science 261:1047–1051
9. Durham HD, Roy J, Dong L, Figlewicz DA (1997) Aggregation of mutant Cu/Zn superoxide dismutase proteins in a culture model of ALS. J Neuropathol Exp Neurol 56(5):523–530
10. Fischer LR, Culver DG, Tennant P, Davis AA, Wang M, Castellano-Sanchez A, Khan J, Polak MA, Glass JD (2004) Amyotrophic lateral sclerosis is a distal axonopathy: evidence in mice and man. Exp Neurol 185:232–240
11. Guegan C, Vila M, Rosoklija G, Hays AP, Przedborski S (2001) Recruitment of the mitochondrial-dependent apoptotic pathway in amyotrophic lateral sclerosis. J Neurosci 21:6569–6576
12. Gurney ME, Pu H, Chiu AY, Dal Canto MC, Polchow CY, Alexander DD, Caliendo J, Hentati A, Kwon YW, Deng HX, Chen W, Zhai P, Sufit RL, Siddique T (1994) Motor neuron degeneration in mice that express a human Cu, Zn superoxide dismutase mutation. Science 264:1772–1775
13. Haenggeli C, Kato AC (2002) Differential vulnerability of cranial motoneurons in mouse models with motor neuron degeneration. Neurosci Lett 335:39–43
14. Higgins CMJ, Jung C, Xu Z (2003) ALS-associated mutant $SOD1^{G93A}$ causes mitochondrial vacuolation by expansion of the intermembrane space and by involvement of SOD1 aggregation and peroxisomes. BMC Neurosci 4:16
15. Hirano A, Kurland LT, Sayre GP (1967) Familial amyotrophic lateral sclerosis. A subgroup characterized by posterior and spinocerebellar tract involvement and hyaline inclusions in the anterior horn cells. Arch Neurol 16:232–243
16. Howland DS, Jiu J, She Y, Goad B, Maragakis NJ, Kim B, Erickson J, Kulik J, DeVito L, Psaltis G, DeGennaro LJ, Cleveland DW, Rothstein JD (2002) Focal loss of the glutamate transporter EAAT2 in a transgenic rat model of SOD1 mutant-mediated amyotrophic lateral sclerosis (ALS). Proc Natl Acad Sci USA 99:1604–1609
17. Inoue K, Fujimura H, Ogawa Y, Satoh T, Shimada K, Sakoda S (2002) Familial amyotrophic lateral sclerosis with a point mutation (G37R) of the superoxide dismutase 1 gene: a clinicopathological study. Amyotroph Lateral Scler Other Motor Neuron Disord 3:244–247
18. Jaarsma D, Haasdijk ED, Grashorn JAC, Hawkins R, Dujin WV, Verspaget HW, London J, Holstege JC (2000) Human Cu/Zn superoxide dismutase (SOD1) overexpression in mice causes mitochondrial vacuolization, axonal degeneration, and premature motoneuron death and accelerates motoneuron disease in mice expressing a familial amyotrophic lateral sclerosis mutant SOD1. Neurobiol Dis 7:623–643
19. Jaarsma D, Rognoni F, Duijn WV, Verspaget HW, Haasdijk ED, Holstege JC (2001) CuZn superoxide dismutase (SOD1) accumulates in vacuolated mitochondria in transgenic mice expressing amyotrophic lateral sclerosis-linked SOD1 mutations. Acta Neuropathol 102:293–305
20. Johnston JA, Ward CL, Kopito RR (1998) Aggresomes: a cellular response to misfolded proteins. J Cell Biol 143:1883–1898
21. Johnston JA, Dalton MJ, Gurney ME, Kopito RR (2000) Formation of high molecular weight complexes of mutant Cu,Zn-superoxide dismutase in a mouse model for familial amyotrophic lateral sclerosis. Proc Natl Acad Sci USA 97:12571–12576
22. Kato S, Takikawa M, Nakashima K, Hirano A, Cleveland DW, Kusaka H, Shibata N, Kato M, Nakano I, Ohama E (2000) New consensus research on neuropathological aspects of familial amyotrophic lateral sclerosis with superoxide dismutase 1 (SOD1) gene mutations: inclusions containing SOD1 in neurons and astrocytes. Amyotroph Lateral Scler Other Motor Neuron Disord 1:163–184
23. Kato S, Horiuchi S, Liu J, Cleveland DW, Shibara N, Nakashima K, Nagai R, Hirano A, Takikawa M, Kato M, Nakano I, Ohama E (2000) Advanced glycation endproduct-modified superoxide dismutase-1 (SOD1)-positive inclusions are common to familial amyotrophic lateral sclerosis patients with SOD1 gene mutations and transgenic mice expressing human SOD1 with a G85R mutation. Acta Neuropathol 100:490–505
24. Kato S, Sumi-Akamaru H, Fujimura H, Sakoda S, Kato M, Hirano A, Takikawa M, Ohama E (2001) Copper chaperone for superoxide dismutase co-aggregates with superoxide dismutase 1 (SOD1) in neuronal Lewy body-like hyaline inclusions: an immunohistochemical study on familial amyotrophic lateral sclerosis with SOD1 gene mutation. Acta Neuropathol 102:233–238
25. Kato S, Saeki Y, Aoki M, Nagai M, Ishizaki A, Itoyama Y, Kato M, Asayama K, Awaya A, Hirano A, Ohama E (2004) Histological evidence of redox system breakdown caused by superoxide dismutase 1 (SOD1) aggregation is common to SOD1-mutated motor neurons in humans and animal models. Acta Neuropathol 107:149–158
26. Klivenyi P, Ferrante RJ, Mathews RT, Bogdanov MB, Klein AM, Andreassen OA, Mueller G, Wermer M, Kaddurah-Daouk R, Flint Beal M (1999) Neuroprotective effects of creatine in a transgenic animal model of amyotrophic lateral sclerosis. Nat Med 5:347–351
27. Kluck RM, Bossy-Wetzel E, Green DR, Newmeyer DD (1997) The release of cytochrome *c* from mitochondria: a primary site for Bcl-2 regulation of apoptosis. Science 275:1132–1136
28. Kong J, Xu Z (1998) Massive mitochondrial degeneration in motor neurons triggers the onset of amyotrophic lateral sclerosis in mice expressing a mutant SOD1. J Neurosci 18(9):3241–3250
29. Liu X, Kim CN, Yang J, Jemmerson R, Wang X (1996) Induction of apoptotic program in cell-free extracts: requirement for dATP and cytochrome *c*. Cell 86:147–157
30. McHanwell S, Biscoe TJ (1981) The sizes of motoneurons supplying hindlimb muscles in the mouse. Proc R Soc Lond 213:201–216
31. Mohajeri MH, Figlewicz DA, Bohn MC (1998) Selective loss of α motoneurons innervating the medial gastrocnemius muscle in a mouse model of amyotrophic lateral sclerosis. Exp Neurol 150:329–336
32. Nagai M, Aoki M, Miyoshi I, Kato M, Pasinelli P, Kasai N, Brown RH Jr, Itoyama Y (2001) Rats expressing human cytosolic copper-zinc superoxide dismutase transgenes with amyotrophic lateral sclerosis: associated mutations develop motor neuron disease. J Neurosci 21(23):9246–9254
33. Nagano S, Ogawa Y, Yanagihara T, Sakoda S (1999) Benefit of a combined treatment with trientine and ascorbate in familial amyotrophic lateral scledosis model mice. Neurosci lett 265:159–162

34. Nagano S, Satoh M, Sumi H, Fujimura H, Tohyama C, Yanagihara T, Sakoda S (2001) Reduction of metallothioneins promotes the disease expression of familial amyotrophic lateral sclerosis mice in a dose-dependent manner. Eur J Neurosci 13:1363–1370
35. Nimchinsky EA, Young WG, Yeung G, Shah RA, Gordon JW, Bloom FE, Morrison JH, Hof PR (2000) Differential vulnerability of oculomotor, facial, and hypoglossal nuclei in G86R superoxide dismutase transgenic mice. J Comp Neurol 416:112–125
36. Olanow CW, Perl DP, DeMartino GN, McNaught KSP (2004) Lewy-body formation is an aggresome-related process: a hypothesis. Lancet Neurol 3:496–503
37. Paxinos G, Franklin KBJ (2001) The mouse brain in stereotaxic coordinates second edition. Academic Press, Figs 79–85
38. Reed JC (1997) Cytochrome *c*: can't live with it-can't live without it. Cell 91:559–562
39. Ripps ME, Huntley GW, Hoff PR, Morrison JH, Gordon JW (1995) Transgenic mice expressing an altered murine superoxide dismutase gene provide an animal model of amyotrophic lateral sclerosis. Proc Natl Acad Sci USA 92:689–693
40. Rosen DR, Siddique T, Patterson D, Figlewicz DA, Sapp P, Hentati A, Donaldson D, Goto J, O'Regan JP, Deng H-X, Rahmani Z, Krizus A, Mckenna-Yasck D, Cayabyab A, Gaston SM, Berger R, Tanzi RE, Halperin JJ, Herzfeldt B, Van den Bergh R, Hung W-Y, Bird T, Deng G, Mulder DW, Smyth C, Laing NG, Soriano E, Pricak-Vance MA, Haines J, Rouleau GA, Gusella JS, Horritz HR, Brown RH (1993) Mutations in Cu/Zn superoxide dismutase gene are associated with familial amyotrophic lateral sclerosis. Nature 362:59–62
41. Sasaki S, Ohsawa Y, Yamane K, Sakuma H, Shibata H, Nakano R, Kikugawa K, Mizutani T, Tsuji S, Iwata M (1998) Familial amyotrophic lateral sclerosis with widespread vacuolation and hyaline inclusions. Neurology 51:871–873
42. Sasaki S, Warita H, Abe K, Iwata M (2004) Slow component of axonal transport is impaired in the proximal axon of transgenic mice with G93A mutant SOD1 gene. Acta Neuropathol 107:452–460
43. Sasaki S, Warita H, Murakami T, Abe K, Iwata M (2004) Ultrastructural study of mitochondria in the spinal cord of transgenic mice with a G93A mutant SOD1 gene. Acta Neuropathol 107:461–474
44. Shibata N, Hirano A, Kobayashi M, Siddique T, Deng HX, Hung WY, Kato T, Asayama K (1996) Intense superoxide dismutase-1 immunoreactivity in intracytoplasmic hyaline inclusions of familial amyotrophic lateral sclerosis with posterior column involvement. J Neuropathol Exp Neurol 55:481–490
45. Shimizu S, Narita M, Tsujimoto Y (1999) Bcl-2 family proteins regulate the release of apoptogenic cytochrome *c* by the mitochondrial channel VDAC. Nature 399:486–487
46. Stathopulos PB, Rumfeldt JAO, Scholzs GA, Irani RA, Frey HE, Hallewell RA, Lepock JR, Meiering EM (2003) Cu/Zn superoxide dismutase mutants associated with amyotrophic lateral sclerosis show enhanced formation of aggregates in vitro. Proc Natl Acad Sci USA 100(12):7021–2026
47. Steiber A, Gonatas JO, Gonatas NK (2000) Aggregation of ubiquitin and a mutant ALS-linked SOD1 protein correlate with disease progression and fragmentation of the Golgi apparatus. J Neurol Sci 173:53–62
48. Stephens B, Navarrete R, Guiloff RJ (2001) Ubiquitin immunoreactivity in presumed spinal interneurons in motor neurone disease. Neuropathol Appl Neurobiol 27:352–361
49. Sugai F, Yamamoto Y, Miyaguchi K, Zhou Z, Sumi H, Hamasaki T, Goto M, Sakoda S (2004) Benefit of valproic in suppressing disease progression of ALS model mice. Eur J Neurosci 20:3179–3183
50. Tsukihara T, Aoyama H, Yamashita E, Tomizaki T, Yamaguchi H, Shinzawa-Itoh K, Nakashima R, Yaono R, Yoshikawa S (1996) The whole structure of the 13-subunit oxidized cytochrome *c* oxidase at 2.8A. Science 272:1136–1144
51. Turner BJ, Lopes EC, Cheema SS (2003) Neuromuscular accumulation of mutant superoxide dismutase 1 aggregates in a transgenic mouse of familial myotrophic lateral sclerosis. Neurosci Lett 350:132–136
52. Turner BJ, Atkin JD, Farg MA, Zang DW, Rembach A, Lopes EC, Patch JD, Hill AF, Cheema SS (2005) Impaired extracellular secretion of mutant superoxide dismutase 1 associates with neurotoxicity in familial amyotrophic lateral sclerosis. J Neurosci 25:108–117
53. Urushitani M, Kurisu J, Takahashi R (2002) Proteasomal inhibition by misfolded mutant superoxide dismutase 1 induces selective motor neuron death in familial amyotrophic lateral sclerosis. J Neurochem 83:1030–1042
54. Wang J, Xu G, Borchelt DR (2002) High molecular weight complexes of mutant superoxide dismutase 1: age-dependent and tissue specific accumulation. Neurobiol Dis 9:139–148
55. Watanabe M, Dykes-Hoberg M, Culotta VC, Price DL, Wong PC, Rothstein JD (2001) Histological evidence of protein aggregation in mutant SOD1 transgenic mice and in amyotrophic lateral sclerosis neural tissues. Neurobiol Dis 8:933–941
56. Wong PC, Pardo CA, Borchelt DR, Lee MK, Copeland NG, Jenkins NA, Sisodia SS, Cleveland DW, Price DL (1995) An adverse property of a familial ALS-linked SOD1 mutation causes motor neuron disease characterized by vacuolar degeneration of mitochondria. Neuron 14:1105–1116
57. Yamashita S, Mita S, Kato S, Okado H, Ohama E, Uchino M (2003) Bcl-2 expression using retrograde transporter of adenoviral vectors inhibits cytochrome *c*-release and caspase-1 activation in motor neurons of mutant superoxide dismutase 1 (G93A) transgenic mice. Neurosci Lett 350:17–20
58. Yang J, Liu X, Bhalla K, Kim CN, Ibrado AM, Cai J, Peng TI, Jones DP, Wang X (1997) Prevention of apoptosis by Bcl-2: release of cytochrome *c* from mitochondria blocked. Science 275:1129–1132

RESEARCH LETTER

Increase of Disease Duration of Amyotrophic Lateral Sclerosis in a Mouse Model by Transgenic Small Interfering RNA

Many lines of evidence show that mutant *SOD1* in familial amyotrophic lateral sclerosis (ALS) gains a novel toxic property, causing neuronal cell death.[1] A simple and attractive therapeutic approach, therefore, is to inhibit the expression of mutant *SOD1*. Small interfering RNA (siRNA) can strongly suppress expression of the target gene and become a powerful tool in gene therapy for dominantly inherited neurodegenerative diseases.[2] Recently, we reported that the onset of ALS symptoms was extremely delayed in SOD1^{G93A} transgenic (Tg) mice when crossed with the Tg mouse overexpressing siRNA to *SOD1*.[3] Here, we furthermore found that this transgenic siRNA could markedly slow the progression of the disease as well.

Methods. We designed the siRNA (GGUGGAAUGAAGAAAGUAC of the sense sequence) as a good and common target region of siRNA to human and mouse *SOD1* messenger RNA.[4] By overexpressing this siRNA with mismatch mutations, we developed the anti-*SOD1* siRNA Tg mouse as previously reported.[3] Briefly, an anti-*SOD1* short hairpin RNA (shRNA) construct was made using human U6 promoter and UUCAAGAGA as a loop sequence. This shRNA expression vector was introduced to mouse ES cells, and the selected ES clone with an approximately 80% reduced level of endogenous *SOD1* was injected into C57BL/6 blastocysts. The resulting chimeric male mouse was mated with C57BL/6, and germline transmission of the shRNA was confirmed. Furthermore, this anti-*SOD1* siRNA Tg mouse was mated with SOD1^{G93A} Tg mice (G1H line from Jackson Laboratories Bar Harbor, Me, backcrossed to C57BL/6 mice) to generate the double Tg mice.

Protein samples were extracted from whole spinal cords; the medial one third of the frontal cortex, including motor cortex; and other areas of cerebral cortex from 3 double Tg mice and 3 SOD1^{G93A} Tg mice. The samples were homogenized in buffer containing 0.1% sodium dodecyl sulfate (SDS), 1% Triton X-100, 1% sodium deoxycholate, and 1mM phenylmethanesulfonyl fluoride. Equal amounts of extracted protein were mixed with Laemmli sample buffer (BioRad, Hercules, Calif), denatured, and separated on 15% SDS polyacrylamide gel electrophoresis. Following transfer onto a polyvinylidene fluoride membrane (BioRad), blots were probed with anti-*SOD1* polyclonal antibody S-100 (Stressgen Biotechnologies, San Diego, Calif). The amount of *SOD1* protein level was estimated by band signal intensity with standard recombinant human *SOD1* (Wako, Tokyo, Japan).

For measuring enzymatic activity, a half of whole brain was homogenized in 5-volume (weight-volume ratio) homogenizing buffer (0.25 M sucrose; 10 mM Tris-hydrochloric acid, pH 7.4; 1 mM ethylenediaminetetraacetic acid). The homogenate was centrifuged at 78 000 g for 60 minutes and the supernatant was removed and saved. Copper-zinc superoxide dismutase activity was measured according to the manufacturer's instruction (SOD Assay Kit–WST; Dojindo Molecular Technologies, Inc, Tokyo).

For immunohistochemical analysis, the lumbar segments of the spinal cords were removed and fixed in 4% paraformaldehyde in phosphate-buffered saline (pH 7.4). The sections (10-μm thick) of the spinal cord at the level of the third lumbar (L3) vertebra were incubated with anti-*SOD1* polyclonal antibody S-100 (1:1000 to 1:15 000, Stressgen Biotechnologies). Staining was visualized by diaminobenzidine.

Results. The crossed double Tg mice had much reduced expression of mutant *SOD1* protein in the multiple areas of the nervous system compared with that in SOD1^{G93A} Tg littermates; the mean±SD *SOD1* protein contents of frontal cortex, including motor cortex; the other area of cerebral cortex; and spinal cord in SOD1^{G93A} Tg mice and double Tg mice were 2.48±0.36, 2.75±0.15, and 3.63±0.26 and 0.84±0.16, 1.03±0.20, and 1.44±0.34 mg per gram of tissue (mean reduction rate, 66.0%, 62.4%, and 69.8%, respectively). The mean±SD enzymatic activity of *SOD1* in SOD1^{G93A} Tg mice and double Tg mice brain was 527.0±22.8 and 172.3±36.3 U/mg, respectively (mean reduction rate, 67.3%). On immunohistochemical analysis, there was no remarkable difference in the *SOD1* immunoreactivity of motor and sensory neurons in the spinal cord of double Tg mice (data not shown).

The double Tg mice showed ALS symptoms after about 10 months old. The symptoms of the double Tg mice were almost same as those of SOD1^{G93A} Tg mice (hind-limb paresis and muscle atrophy, lack of mobility followed by breathing difficulties) except for lack of tremor. Onset of motor function loss was observed at a mean±SD age of 358.6±41.0 days (range, 302-520 days) in the double Tg mice (n=5) and 127.3±1.2 days (range, 115-135 days) in SOD1^{G93A} Tg mice (n=23) (difference, P=.003 by log-rank test). The mean±SD survival time was also much prolonged in the double Tg mice (395.2±45.3 days; range, 326-574 days) compared with that in SOD1^{G93A} Tg mice (145.9±1.7 days; range, 130-157 days) (difference, P=.003). Most importantly, the disease progression of

limb weakness was markedly slowed and the duration from onset of the hind-limb dysfunction to death was significantly prolonged in the double Tg mice compared with that in the $SOD1^{G93A}$ Tg mice (double Tg mice, 36.6±5.7 days; $SOD1^{G93A}$ Tg mice, 18.6±1.6 days; $P=.02$).

Comment. In the previous reports in which siRNA-expressing lentivirus[5] or adeno-associated[6] virus was injected to muscles of $SOD1^{G93A}$ Tg mice, the onset of weakness was markedly delayed,[5,6] but disease progression did not significantly change.[5] In another report[7] in which siRNA-expressing lentivirus was injected to lumbar spinal cord of $SOD1^{G93A}$ Tg mice, the onset and progression of the hind-limb dysfunction were delayed, but the disease duration was not described. In these reports, siRNA did not reach all motoneuron innervating bulbar and respiratory muscles of which paresis should influence the life span of this ALS mouse model. In contrast, all motoneurons and glial cells throughout the central nervous system in our crossed double Tg mice had siRNA expressed by the shRNA transgene. Therefore, our study is considered to be better than the other 3 reports in evaluating the siRNA effect on the disease duration after the onset until death. We clearly proved that siRNA-mediated gene silencing can slow the disease progression and increase the disease duration of ALS in a mouse model, suggesting that treatment with siRNA after the onset of disease is beneficial for slowing down the progression and expanding the life span of patients with this fatal disease.

Takanori Yokota, MD, PhD
Hiroki Sasaguri, MD
Yuki Saito, MD, PhD
Hiromi Yamada
Toshinori Unno
Yuki Yamamoto
Takayuki Kubodera, MD, PhD
Masayuki Anzai, PhD
Tasuku Mitani, PhD
Hidehiro Mizusawa, MD, PhD

Correspondence: Dr Yokota, Department of Neurology and Neurological Science, Tokyo Medical and Dental University, 1-5-45 Yushima Bunkyo-ku, Tokyo 113-8519, Japan (tak-yokota.nuro@tmd.ac.jp).

Author Contributions: *Study concept and design:* Yokota. *Acquisition of data:* Yokota, Sasaguri, Saito, Yamada, Unno, Yamamoto, Kubodera, Anzai, and Mitani. *Analysis and interpretation of data:* Yokota. *Drafting of the manuscript:* Yokota and Mitani. *Critical revision of the manuscript for important intellectual content:* Yokota, Sasaguri, Saito, Yamada, Unno, Yamamoto, Kubodera, Anzai, and Mitani. *Statistical analysis:* Yokota. *Obtained funding:* Yokota, Sasaguri, Saito, Yamada, Unno, Yamamoto, Kubodera, Anzai, and Mitani. *Administrative, technical, and material support:* Yokota. *Study supervision:* Yokota and Mizusawa.
Financial Disclosure: None reported.
Funding/Support: This study was supported by grants from the Ministry of Education, Science, and Culture; the Ministry of Health, Labor, and Welfare; the Nakabayashi Trust for Amyotrophic Lateral Sclerosis Research; and the Kato Memorial Bioscience Foundation.

1. Cleveland DW. From Charcot to SOD1: mechanisms of selective motor neuron death in ALS. *Neuron.* 1999;24:515-520.
2. Davidson BL, Paulson HL. Molecular medicine for the brain: silencing of disease genes with RNA interference. *Lancet Neurol.* 2004;3:145-149.
3. Saito Y, Yokota T, Mitani T, et al. Transgenic small interfering RNA halts amyotrophic lateral sclerosis in a mouse model. *J Biol Chem.* 2005;280:42826-42830.
4. Yokota T, Miyagishi M, Hino T, et al. siRNA-based inhibition specific for mutant SOD1 with single nucleotide alternation in familial ALS, compared with ribozyme and DNA enzyme. *Biochem Biophys Res Commun.* 2004;314:283-291.
5. Ralph GS, Radcliffe PA, Day DM, et al. Silencing mutant SOD1 using RNAi protects against neurodegeneration and extends survival in an ALS model. *Nat Med.* 2005;11:429-433.
6. Miller TM, Kaspar BK, Kops GJ, et al. Virus-delivered small RNA silencing sustains strength in amyotrophic lateral sclerosis. *Ann Neurol.* 2005;57:773-776.
7. Raoul C, Abbas-Terki T, Bensadoun JC, et al. Lentiviral-mediated silencing of SOD1 through RNA interference retards disease onset and progression in a mouse model of ALS. *Nat Med.* 2005;11:423-428.

Guidelines for Letters

Letters discussing a recent *Archives of Neurology* article will have the best chance of acceptance if they are received within 4 weeks of the article's publication date. They should not exceed 400 words of text and 5 references. Letters reporting original research should not exceed 600 words and 6 references. All letters should include a word count. Letters must not duplicate other material published or submitted for publication. Letters will be published at the discretion of the editors and are subject to editing and abridgment. A signed statement for authorship criteria and responsibility, financial disclosure, copyright transfer, and acknowledgment is required for publication. Letters not meeting these specifications are generally not considered. Before submitting a Research Letter, please review the Instructions for Authors (September 2004 or http://archneur.ama-assn.org/misc/ifora.dtl).